

Received March 24, 2020, accepted April 11, 2020, date of publication May 6, 2020, date of current version May 21, 2020.

Digital Object Identifier 10.1109/ACCESS.2020.2992913

# Development of GaN Technology-Based DC/DC Converter for Hybrid UAV

JUANA M. MARTÍNEZ-HEREDIA<sup>1</sup>, (Member, IEEE), FRANCISCO COLODRO<sup>1</sup>,  
JOSÉ LUIS MORA-JIMÉNEZ<sup>1</sup>, ALEJANDRO REMUJO<sup>1</sup>, JOAQUÍN SORIANO<sup>1</sup>,  
AND SERGIO ESTEBAN<sup>2</sup>

<sup>1</sup>Department of Electronic Engineering, University of Seville, 41092 Seville, Spain

<sup>2</sup>Department of Aerospace Engineering, University of Seville, 41092 Seville, Spain

Corresponding author: Juana M. Martínez-Heredia (jmmh@us.es)

This work was supported by the Spanish Ministry of Science, Innovation and Universities under Project RTI2018-101519-A-I00.

**ABSTRACT** Wide band-gap (WBG) semiconductors technology represents a potential candidate to displace conventional silicon (Si) technology used in power electronics. Between Silicon Carbide (SiC) and Gallium Nitride (GaN) power semiconductors, the latter is the least mature of both technologies, with many open research problems, especially in the aerospace industry. In this paper, we address the design and implementation of a DC/DC converter for a hybrid small unmanned aerial vehicle (UAV) based on GaN technology. Both theoretical and simulation comparisons of Si, SiC and GaN transistors for the converter are presented. The conclusion is that GaN devices are the most appropriate to fulfill converter requirements for the size and weight limitations of the selected UAV. The paper presents a buck converter which handles an input voltage range of 32 V to 40 V and provides a 12 V regulated output and output power up to 60 W. The experimental results carried out on the prototype converter show how promising the GaN technology is for aerospace systems, not only regarding its volume and size, but also its efficiency. Besides, practical implementation details are reported to contribute to the design of small, light and reliable GaN power converters for aeronautics.

**INDEX TERMS** Aerospace electronics, DC-DC power converters, Gallium Nitride (GaN) transistors, wide band-gap (WBG) semiconductors, unmanned aerial vehicle (UAV).

## I. INTRODUCTION

Traditionally, unnamed aerial vehicles (UAVs) have been used worldwide for military purposes. However, in the last decade, commercial and civilian usage of drones has rapidly increased. According to experts, the market for commercial and civilian drones will grow at a higher rate than the military ones in the coming years. In particular, the Federal Aviation Administration (FAA) estimates that more than 7 million small hobbyist and commercial UAVs are expected to be purchased by 2020 with 6.1 million sales for 2019 [1]. Drones have multiple civil uses such as search and rescue operations, surveillance, forest fire detection, package delivery, pollution and environmental monitoring, reconnaissance operations, or precision crop monitoring.

Miniaturization and innovation of electronics [2] is one of the technological drivers that can transform UAV industry:

The associate editor coordinating the review of this manuscript and approving it for publication was Jiankang Zhang<sup>1</sup>.

it will allow reducing the drone's overall weight and size, while improving efficiency. Small drones are often powered by lithium-ion and lithium polymer rechargeable batteries, but recently efforts have been made to extend the duration of the missions by using a combination of hybrid power sources, like fuel cells, batteries or solar cells [3]–[6]. This hybridization of different power sources with different power outputs requires an appropriate DC/DC converter. As the rest of electrical and electronic equipment on board of the UAV, this power converter must be as small, light and energetically efficient as possible, which poses a true technological challenge.

The aim of this paper is to propose a DC/DC converter suitable for a hybrid UAV. This convertible UAV is currently being developed by a working team formed by researchers from several Spanish and Brazilian universities in collaboration with partners of the emergency medical care service (SAMU). The power converter must meet the desirable requirements of small size and weight while maximizing

its energy efficiency. For this purpose, we investigated several emergent technologies in power electronics: wide band-gap (WBG) semiconductors as Silicon Carbide (SiC) and Gallium Nitride (GaN) [7]–[11]. Furthermore, we evaluated the advantages and disadvantages of its utilization in the area of small drones paying special attention to the feasibility of our proposal.

This paper is organized as follows. Section II exposes the system requirements for the DC/DC converter that will be on board of the UAV currently under development. Section III reminds the principles of operation and design of the proposed buck converter. The main contributions of this paper are presented in the following sections: Section IV presents the result of comparing Si, SiC and GaN power transistors. Section V provides the experimental setup and results of the GaN-based converter along with a discussion on them. Finally, section VI presents the conclusions and future work.

## II. DC/DC CONVERTER REQUIREMENTS FOR HYBRID UAV

Emerging technologies are radically changing traditional operating procedures in disaster relief and emergency response management. In particular, UAVs or also known as Remotely Piloted Aircraft System (RPAS), for those operated remotely, are proving themselves extremely useful in Search And Rescue (SAR) missions. They bring very advantageous capabilities such as rapid response, remote operation, transportation of equipment, monitoring of wide areas, and multi-sensor deployment.

Rapid Intervention Vehicles (RIV) typically used in SAR missions have cargo space for at most one small RPAS of either fixed or rotary wing type. Fixed wing aircrafts are well suited for rapid deployment and remote monitoring but they require external means (runways or catapults) for takeoff and landing, and they cannot hover. Rotary wing aircrafts (such as quadrotors) have much less autonomy and range but they can hover and perform Vertical Take-Off and Landing (VTOL); thus, they are suited for restricted or inaccessible areas and sensor deployment. A third kind of aircraft, still relatively uncommon, is fixed-wing convertible aircraft with VTOL capabilities [12]. They have the advantages of fixed and rotary wing aircraft without most of their shortcomings. A convertible UAV would allow a first response RIV to operate a single multi-purpose, multi-mission aircraft.

The UAV that is being developed is proposed to explore the use of convertible fixed-wing aircraft with VTOL capability specifically designed for SAR missions. The aircraft will be easy to operate and fast to deploy; to this mean, guidance, navigation and control algorithms will be developed considering the requirements of SAR missions. Besides, highly integrated and efficient embedded electronics will be developed to reduce the aircraft dimensions and increase its autonomy. Autonomy will be increased through use and management of renewable power sources such as solar and fuel cells. The interdisciplinary nature of this project guarantees its novelty and the different technologies that will be developed ensure a breakthrough in the way that UAVs are used in emergencies:



**FIGURE 1. Partial result achieved in the development of the convertible UAV: scale model in wind tunnel.**

currently, they only use either fixed wing or rotary wing technology due to the complexity and high-risk associated to develop this technology.

The first studies conducted (last 4 years) in this field by the research team ([13], [14]) jointly with companies in the emergency sector have determined that for maximum use the aircraft should have the following characteristics:

- Small dimensions, so that it can be transported in a rapid intervention vehicle (VIR) for its integration into the coordinated rapid response measures in emergency situations.
- Versatility to carry out a variety of SAR missions, from monitoring to surveillance, transportation of diverse medical payloads, or deployment of sensors, with the greatest autonomy and scope possible.
- Simplicity and secure operation so that even a health-care professional can use it with hardly any additional training.
- Compliance with airworthiness requirements.

Based on the established requirements, a series of work packages have been created that mark the development of the aircraft following a bottom up sequential design with concurrent engineering interaction between all the involved packages. One of the work packages is the development of high efficiency embedded electronic systems, in which this paper is motivated. Fig. 1 shows an example of partial result achieved to date: a scale model of the UAV-VTOL implemented to be tested in a wind tunnel.

Some of the characteristics of UAVs such as weight (19 kg including structure, avionics, payload, and power sources) and size (wingspan of 2.26 m and a fuselage length of 1.67 m) will impose requirements on the weight and size of the electronic systems to be developed and integrated into the aircraft.

Previous studies in the field of generation and storage of energy in the convertible UAV have established that the power supply to the engines and systems will be given by a hybrid system of hydrogen fuel cells, batteries and solar panels. This system, whose objective is to reach the optimum degree of hybridization to maximize the drone performance, will give a rated output voltage of 36 V which must be transformed through various power converters with the ultimate goal of

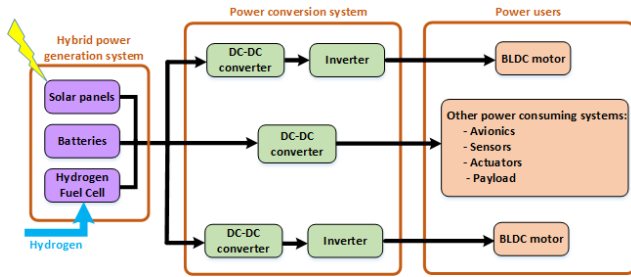


FIGURE 2. Scheme of the electrical system of the UAV under development.

feeding the different users on board such as motors, computers, actuators, and sensors. Fig. 2 shows a general description of the components that make up the electrical system of the convertible UAV under development. The power conversion system is made up of a DC-DC power converter plus an inverter to power each brushless DC electric motor of the UAV and a DC-DC converter for the rest of equipment. This work focuses on the DC-DC converter which will provide the supply voltage to the rest of the UAV’s electronic systems. Thus, this converter must be capable of providing the voltages required for the possible subsystems that will go embarked on the UAV while delivering enough power for optimum operation. Other design objectives will be high efficiency and a reduced weight and size.

Previous studies determined that with the avionics and payload that the convertible UAV would carry, it would be required a DC/DC converter able to deliver 12 V and 60 W to a load. Its input voltage can range from 32 V to 40 V, being 36V the rated input voltage. Other general requirements for the converter are:

- Load regulation and line regulation must be comparable to those in similar commercial converters (between 0.5% and 3%, approximately).
- It must be very efficient compared with silicon-based converters (these present a peak efficiency ranging from 86% to 92%).
- It must be light enough; we think a good design would have a weight less than 1% of the weight of the UAV.
- It must be small enough to be mounted inside the UAV fuselage together with the payload. The maximum total volume of the system will depend strongly on the model of UAV to use.

In this paper, as reference mission profile for this class of UAV, we consider a 19 kg MTOW (maximum take-off weight) airplane cruising at 300 m AGL (above ground level). So, the maximum weight of the converter must be 190 g. Besides, since the variety of UAV fuselages existing nowadays, we estimate a maximum volume of the converter of 6 cm × 3 cm × 2 cm.

### III. PRINCIPLES OF OPERATION AND DESIGN OF A BUCK CONVERTER

Since we require a DC/DC converter with very high efficiency, it is necessary to choose a switching regulator design

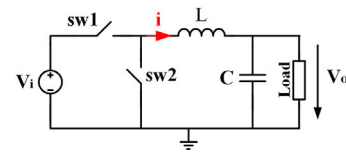


FIGURE 3. Scheme of the ideal buck converter.

versus a linear regulator. In order to provide the 12 V output from the input range [32 V, 40 V] we have chosen a classical non-isolated topology because of its simplicity and its well-known efficiency: a step-down (buck) converter. Fig. 3 shows this topology where all the components (switches sw1 and sw2, inductor L and capacitor C) are assumed ideal. We have considered that our converter does not require electrical isolation between the input and output. Thus, we do not have to use a transformer to eliminate the dc path between its input and output, reducing the complexity, the number of components and the size of the converter.

Although the aim of this paper is to study the impact of emergent devices on power converters for small drones (size, weight, switching losses, etc), this section presents a summary of the operating principles of the converter for those readers who are not familiar with power electronics.

Operation of the buck converter is based in two stages: the ON and OFF stages. In the ON stage, with duration  $t_{on}$ , the switch sw1 is closed and the switch sw2 is open. Then the current flows from the source  $V_i$  towards the load, through the inductor  $L$ , and it will go increasing. The voltage induced across the inductor will counteract the voltage of the source and will reduce the output voltage. At the same time, the inductor will store energy in the form of a magnetic field. In the OFF stage, with duration  $t_{off}$ , the switch sw1 is open and the switch sw2 is closed. Then the source voltage  $V_i$  is disconnected from the circuit but the current  $i$  through the inductor will continue to flow due to the switch sw2, which is closed. The current magnitude will drop and, thus, the induced voltage across the inductor will change its direction. The inductor becomes a source to supply the load by releasing its stored energy.

By switching between on-state and off-state at a constant frequency  $f_s$  (switching time period  $T_s = 1/f_s = t_{on} + t_{off}$ ), the buck converter is able to produce a lower  $V_o$  average voltage than the dc input voltage  $V_i$ . Assuming steady state, the average output voltage is controlled by controlling the switch on and off duration ( $t_{on}$  and  $t_{off}$ ) and can be calculated [13] as

$$V_o = \frac{1}{T_s} \int_0^{T_s} v_o(t) dt = \frac{1}{T_s} \left( \int_0^{t_{on}} V_i dt + \int_{t_{am}}^{T_s} 0 dt \right) = \frac{t_{on}}{T_s} V_i \quad (1)$$

Defining the switch duty cycle  $D$  as the ratio of the on duration to the switching time period ( $D = t_{on}/T_s$ ), (1) yields  $V_o = DV_i$ . So, by varying  $D$ , the output voltage  $V_o$  can be controlled. Besides,  $V_o$  is always less than or equal to the input since  $D$  is between 0 and 1.

The converter can operate in two operating modes: continuous mode (CCM), where the current  $i$  through the inductor is always greater than zero, and discontinuous mode, where  $i$  can be canceled at some point. We have chosen that the converter operates in CCM because the relationship between  $V_o$  and  $V_i$  is linear (it only depends on  $D$ ) and thus, it is easier to control the system.

This method for controlling the output voltage by switching at a constant frequency  $f_s$  and varying the duty cycle is called pulse-width modulation (PWM) switching. We have assumed that our buck converter is asynchronous, that is, its switch  $sw2$  is implemented with a diode and we only need one signal to turn on or turn off the switch  $sw1$ .

For the design of the converter, it is necessary to choose the elements so that the converter's performances could be optimum [15]. For given values of  $T_s$ ,  $V_o$ ,  $V_i$ ,  $L$  and  $D$ , if the average output current through the load  $I_o$  becomes less than a certain critical value  $I_{oc}$ , then the current  $i$  through the inductor will become discontinuous:

$$I_{oc} = \frac{T_s D}{2L} (V_i - V_o) \quad (2)$$

Thus, in order to ensure continuous conduction mode (CCM), the value of the inductor  $L$  must be greater than a critical value  $L_c$  given by

$$L_c = \frac{T_s V_i}{2I_o} D(1 - D) = \frac{V_o(1 - D)}{2f_s I_o} \quad (3)$$

Equation (3) shows that the value of  $L_c$  must also consider the minimum current to be provided by the converter.

Regarding the output capacitor  $C$ , in the previous analysis, it has been assumed to be so large to yield  $v_o(t) = V_o$ . Nevertheless, for a practical value of  $C$ , the ripple in the output voltage can be calculated according to

$$\frac{\Delta V_o}{V_o} = \frac{T_s^2}{8LC} (1 - D) = \frac{\pi^2}{2} (1 - D) \left( \frac{f_c}{f_s} \right)^2 \quad (4)$$

where  $f_c = 1/[2\pi(LC)^{0.5}]$  is the cutoff frequency of the low-pass filter composed by the inductor  $L$  and the capacitor  $C$  of the converter. This filter significantly reduces the output fluctuations by selecting  $f_c \ll f_s$ . As well, (4) shows that the ripple is independent of the output load power in CCM.

We have assumed that the switch  $sw1$ , the diode, the inductor and the capacitor are ideal and they have no associated losses. Furthermore, the power conversion efficiency  $\eta = P_o/P_i$  is unity or 100%.

Nevertheless, real devices have parasitic effects that affect the performances of the converter such as the efficiency, the  $V_o/V_i$  ratio, the peak-peak voltage ripple, etc. So, the real capacitor will have a power loss which can be estimated by multiplying the root mean square (RMS) current through the capacitor by the square of its equivalent series resistance (ESR). Therefore, we must choose this capacitor with ESR as small as possible. In fact, considering the ESR in our converter, the ripple in the output voltage can be

approximated to

$$\frac{\Delta V_o}{V_o} = \max \left[ \frac{T_s^2(1 - D)}{8LC}, \frac{T_s(1 - D)}{L} ESR \right] \quad (5)$$

The real inductor will have losses that will reduce the efficiency and as well, we will have to ensure that it will handle the peak currents of the circuit.

The real diode also presents an energy loss which affects the efficiency and operation of the power converter. The diode energy loss is composed of conduction and switching losses, where the turn-off energy loss is critical. So we could choose a Schottky diode or a fast-recovery diode. Schottky diodes are used in very low output voltage circuits because they have low forward voltage drop (typically 0.3V). Fast-recovery diodes are usually used in high-frequencies circuits.

As to the transistor, which implements the controllable switch  $sw1$  in Fig. 3, it could be a bipolar junction transistor (BJT), a metal-oxide-semiconductor field effect transistor (MOSFET), a gate turn off (GTO) thyristor or an insulated gate bipolar transistor (IGBT). Provided the low value of the currents and voltages of our converter, BJTs and MOSFETs would be more suitable. Moreover, a MOSFET would be a better option than a BJT because of the ease of control, higher switching speed, lower switching power losses, lower on-resistance, and reduced susceptibility to thermal runaway. The choice of this device among the commercially available is extremely important in designing the power electronic converter and it depends strongly on the specific application.

In the last decades one of the main trends to reduce the volume, weight and cost of the power converters has been to increase the switching frequency since it reduces the required size of the passive energy storing elements (inductors and capacitors). However, the increase in switching frequency also increases the switching losses and thus, the efficiency can become poor and the power semiconductors can fail due to overheating. Some methods for decreasing switching losses have been proposed: resonant converters (series, parallel and series-parallel) [15], multilevel converters [16] or new materials for power semiconductors [7], [17]. These materials are Silicon Carbide (SiC) and Gallium Nitride (GaN), both wide band-gap (WBG) semiconductors. Therefore, we have decided to investigate these new technologies of power devices to improve performances as efficiency, size and weight of a conventional power converter and be able to onboard it in the hybrid UAV we are developing.

#### IV. COMPARISON OF Si, SiC AND GaN POWER SWITCHES

In this work we explore the characteristics of real Si, SiC and GaN power switches in order to choose the most appropriate for our converter. First, we carry out a theoretical comparison of Si, SiC and GaN semiconductors and then, a simulation-based comparison of Si, SiC and GaN power switches.

**TABLE 1. Material properties of Si, SiC and GaN.**

Item	Si	4H-SiC	GaN
Band gap energy $E_g$ (eV)	1.12	3.26	3.43
Breakdown field $E_c$ (kV/cm)	300	2200	3300
Saturation velocity $v_{sat}$ (cm/s)	$1 \times 10^7$	$2 \times 10^7$	$2.2 \times 10^7$
Electron Mobility $\mu_n$ (cm <sup>2</sup> /V·s)	1300	950	1500
Hole Mobility $\mu_p$ (cm <sup>2</sup> /V·s)	600	120	350
Dielectric constant $\epsilon_r$	11.8	10	9
Thermal Conductivity $\lambda$ (W/cm·K)	1.5	3.8	1.3

**A. THEORETICAL COMPARISON OF Si, SiC AND GaN SEMICONDUCTORS**

Scientific literature on properties of semiconductor materials has been reviewed and significant variations in some values have been found [8], [17], [18]. In this paper, we present Table 1 as a good comparison among some key properties of the main semiconductors used for high-performance electronics applications.

The main property of WBG semiconductors such as GaN and SiC is that they have higher band gaps than silicon. Thus, they have lower intrinsic leakage currents and can withstand higher operating temperatures than Si.

Other property of GaN and SiC is that they have higher critical or breakdown field than Si, which allows them to operate with higher voltages. Then, in transistors with the same value of breakdown voltage, the layers of devices with GaN and SiC technology can be thinner than those of Si, which means smaller dimensions and higher power density. Besides, GaN has the critical electric field 1.5 times higher than SiC.

The saturation drift velocity (maximum average drift speed that an electron reaches when the applied electric field is greater than a threshold value) is one of the main factors on which the switching capacity of semiconductor devices depends. It is higher in GaN and SiC than in Si. This characteristic, together with a greater mobility of electrons and holes than the SiC, makes the GaN the favorite material for operating at high frequencies.

The thermal conductivity measures the heat conduction capacity of the materials. The evolution of temperature is a critical factor in the operation of semiconductor devices since the increase in temperature means a decrease in the mobility of electrons and therefore, a lower efficiency in operation. In addition, high temperatures can damage the devices and the other component around them. Regarding this issue, the SiC has a clear advantage over Si and GaN. It has a thermal conductivity twice that of Si and GaN, so it shows a superior capacity to transfer heat from the inside of the device to the outside. SiC is the best option for devices that operate at high temperatures.

To facilitate the comparison of the power devices manufactured with different materials, a series of parameters called figures of merit (FOM) have been defined, which summarize some of the main properties of these materials. Some of them are:

- JFOM: it was proposed by Johnson [19] and it estimates the potential of a material for high frequency and high power

applications. For this, it considers the electric breaking field  $E_c$  and the saturation velocity  $v_{sat}$ .

$$JFOM = \frac{E_c v_{sat}}{2\pi} \tag{6}$$

It has a value of about  $1.1 \times 10^{12}$  V/s for silicon.

- KFOM: it was proposed by Keyes [20] and it provides the thermal limitation to the switching behavior of the transistors, considering the thermal conductivity of the semiconductor  $\lambda$ , its dielectric constant  $\epsilon_r$  of the material, the velocity of light in free space  $c$  and the saturation velocity  $v_{sat}$ .

$$KFOM = \lambda \sqrt{\frac{c v_{sat}}{4\pi \epsilon_r}} \tag{7}$$

It has a value of about  $1.17 \times 10^{15}$  W/deg/sec for silicon. The KFOM specifies the maximum switching speed of an electronic logic element.

But these traditional figures of merit (JFOM and KFOM) did not do justice to GaN and SiC versus Si. Neither the application of semiconductor transistor in the final application circuit nor its reliability was considered. So Baliga [21] derived a figure of merit which defines material parameters to minimize the conduction losses in power transistors, considering the electron mobility  $\mu_n$ , the band gap of the semiconductor  $E_g$  and the dielectric constant  $\epsilon_r$  of the material:

$$BFOM = \epsilon_r \mu_n E_g^3 \tag{8}$$

The BFOM is based upon the assumption that the power losses are solely due to the power dissipation in the on-state by current flow through the on-resistance of the power transistor. Thus, the BFOM applies to systems operating at lower frequencies where the conduction losses are dominant. Later, Baliga [22] proposed a new FOM, with dimensions of frequency, for devices operating at high frequencies:

$$BHFFOM = \frac{1}{R_{ON} C_{iss}} = f_B \tag{9}$$

where  $R_{ON}$  and  $C_{iss}$  are the specific on-resistance and capacitance, which are both determined by the material characteristics and the device cell design. In fact, the BHFFOM can be rewritten in terms of the material parameters:

$$BHFFOM = \mu_n E_c^2 V_G^{0.5} / 2BV^{1.5} \tag{10}$$

where  $V_G$  and  $BV$  are the applied gate bias voltage and the breakdown voltage, respectively. The BHFFOM estimates the potential of a material for high power applications and high frequencies where the switching losses due to the charging and discharging of the device become more important.

Table 2 shows the mentioned figures of merit for SiC and GaN normalized with respect to Si [23]. SiC and GaN present better performance for high frequency and high power applications than Si. Moreover, GaN transistors have higher operating efficiency at higher frequencies than SiC transistors; this advantage is reflected in higher values of BFOM and BHFFOM. In any case, although these figures of merit are frequently used, they are approximate estimations of

**TABLE 2. Normalized values of figures of merit for GaN and SiC.**

	JFOM	KFOM	BFOM	BHFFOM
Si	1	1	1	1
4H-SiC	23	3.9	15.3	57-76
GaN	15	1.5	25.3	86-172

the operation of the devices. They do not contemplate the parasitic resistances and other effects that limit their operation. So other figures of merit can be defined to show more effects [24].

**B. SIMULATION-BASED COMPARISON OF Si, SiC AND GaN TRANSISTORS**

In this section, we will perform an analysis by simulation of the behavior of GaN, Si and SiC transistors in order to determine the advantages and disadvantages of the GaN technology. We will study characteristics such as, among others, thermal behavior, energy losses and characteristic curves. This study will be carried out through simulations with the simulation program SPICE from the models provided by the manufacturers.

In order to compare different technologies, it is necessary to choose devices with similar design parameters of drain-source breakdown voltage ( $BV_{DS}$ ), maximum resistance ( $R_{DS(on)}$ ) and maximum continuous drain current ( $I_{DS}$ ). Since the GaN transistors catalog is still reduced, the initial choice will be made on GaN devices and, later, we will choose Si and SiC transistors with similar parameters. We have chosen the transistors shown in Table 3, which have good models of thermal behavior and high-frequency behavior. Simulation results indicate a good agreement with the data provided by datasheets from manufacturers.

These transistors have high breakdown voltages (650 V), maximum continuous drain currents around 30 A (except the model IPB65R190C7, which has 13 A) and resistances  $R_{DS(on)}$  between 50 mΩ and 190 mΩ. We have not found Si and SiC transistors with values of  $R_{DS(on)}$  as small as in the GaN transistors and comparable values of  $I_{DS}$ . Some of the advantages of GaN technology are based on this fact. Besides, one of the advantages of the selected GaN transistor is its small size compared to the other devices. Table 3 shows the dimensions of the transistors obtained from their datasheets. Although the area (width per length) of the GaN and Si transistors is similar, the SiC transistor has an area that triples it. Moreover, the GaN transistor presents a laminated packaging much finer than the usual TO-XX, up to 10 and 20 times smaller in volume.

Despite the IPB65R190C7 Si transistor has a  $R_{DS(on)}$  of 190 mΩ, larger than the rest, it has been included in Table 3 because of its lowest price. But if we choose a Si MOSFET with similar  $R_{DS(on)}$  to a GaN or SiC transistor, its price is not much lower. So, hereinafter, we will only consider the transistors GS66508P (GaN), SCT3080ALGC11 (SiC) and IPB65R065C7 (Si).

Fig.4 shows the simulated gate-to-source threshold voltage ( $V_{GS(th)}$ ) of the chosen transistors depending on the

**TABLE 3. List of transistors to be analyzed and their main parameters.**

Model	GS66508P	SCT3080ALGC11	IPB65R065C7	IPB65R190C7
Material	GaN	SiC	Si	Si
$BV_{DS}$ (V)	650	650	650	650
$I_{DS}$ (A)	30	30	33	13
$R_{DS(on)}$ (mΩ)	50	80	65	190
Price (\$)	26.7	9.8	7.2	2.9
Packaging	GaNXP™	TO-247-3	PG-TO 263	PG-TO 263
Size (mm x mm x mm)	10.0 x 8.7 x 0.51	16.2 x 21.2 x 5.2	10.31 x 9.45 x 4.57	10.31 x 9.45 x 4.57
Volume (mm³)	44.49	1680	445.25	445.25

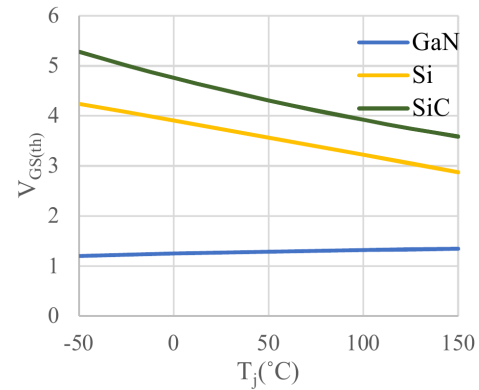


**FIGURE 4.  $V_{GS(th)}$  versus of the junction temperature  $T_j$  for the chosen transistor models (GaN, Si, SiC).**

operating junction temperature ( $T_j$ ), which has been varied from  $-50^\circ\text{C}$  to  $150^\circ\text{C}$ . The GaN transistor keeps the  $V_{GS(th)}$  value relatively constant with temperature: only an increase of 0.15 V is shown. In the case of Si and SiC transistors, it is shown that  $V_{GS(th)}$  decreases about 2 V. In addition, the  $V_{GS(th)}$  values for GaN transistors are much smaller than those of other technologies and this is an advantage to drive the device from microcontrollers with small output voltages (for example, 5 V).

One of the most important parameters of a power transistor is the drain-source on-state resistance  $R_{DS(on)}$ , which determines the conduction losses. Fig. 5 shows the  $R_{DS(on)}$  values (in mΩ) of each chosen device for a specific gate-to-source voltage  $V_{GS}$  and junction temperature values  $T_j$  between  $25^\circ\text{C}$  and  $150^\circ\text{C}$  with an increase of  $25^\circ\text{C}$ . In order to compare more justly the transistors according to the  $R_{DS(on)}$ , we have taken into account the maximum  $V_{GS}$  of each one since it will provide the minimum  $R_{DS(on)}$ : 7 V for the GS66508P, 20 V for the IPB65R065C7 and 22 V for the SCT3080ALGC11. So we have chosen  $V_{GS}$  of 6 V for the GS66508P and 18 V for the IPB65R065C7 and the SCT3080ALGC11. Besides, given that the  $R_{DS(on)}$  decreases if the drain current  $I_{DS}$  increases, we have remarked the value of  $R_{DS(on)}$  for a same value of  $I_{DS}$  (9 A) at  $25^\circ\text{C}$  and  $150^\circ\text{C}$  in all cases. So, if we had chosen  $V_{GS}$  of 6 V for all the transistors, the GaN transistor would be the best regarding to the  $R_{DS(on)}$  (50 mΩ versus 65 mΩ of the Si one and 125 mΩ of the SiC one). However, if we establish fairer conditions to compare them, as said before, we can observe that at  $25^\circ\text{C}$  the GaN transistor keeps the

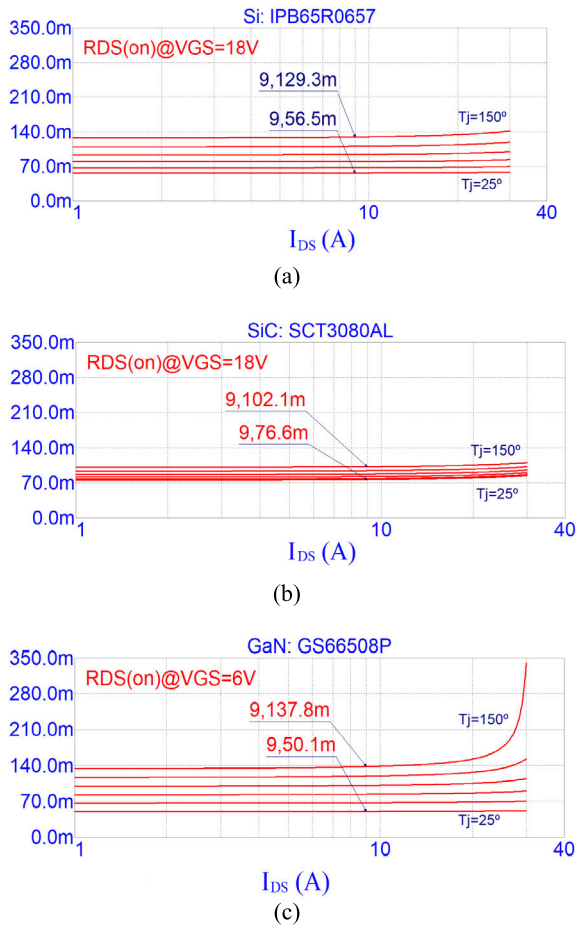


**FIGURE 5.**  $R_{DS(on)}$  versus of the drain current  $I_{DS}$  for different values of the junction temperature  $T_J$  for the chosen transistors: (a) Si, with  $V_{GS} = 18\text{ V}$ , (b) SiC, with  $V_{GS} = 18\text{ V}$ , and (c) GaN, with  $V_{GS} = 6\text{ V}$ .

lowest  $R_{DS(on)}$  (50 m $\Omega$  vs. 56 m $\Omega$  in the Si one and 76 m $\Omega$  in the SiC one) but, for high operation temperatures, it is the SiC transistor which has the lowest  $R_{DS(on)}$  (for example, at 150  $^\circ\text{C}$ , 102 m $\Omega$  vs. 129 m $\Omega$  in the Si one and 137 m $\Omega$  in the GaN one).

We have studied the time evolution of the junction and case temperature for the chosen transistors with and without an external heat sink. A thermal interface material (TIM) has been attached to the heat sink in order to improve heat transfer. We must mention that the manufacturer of the chosen GaN devices implements a new packaging: the discrete device is embedded within a laminate construction so that it leads to smaller volume, lower resistance and lower inductance than a conventional packaging. In the case of the Si device (package TO-263), a heat sink 573300D00010G has been selected. For the SiC device (package TO-247-3), a heat sink R2A-CT4-38E has been selected. And for the GaN device, we have considered the cooling method recommended by the manufacturer for the GaN $PX$  package: a bottom side cooling with a heat sink via a PCB attached to the thermal pad of the device. In this case we have selected a heat sink MPC14-14. Table 4 shows the value of the

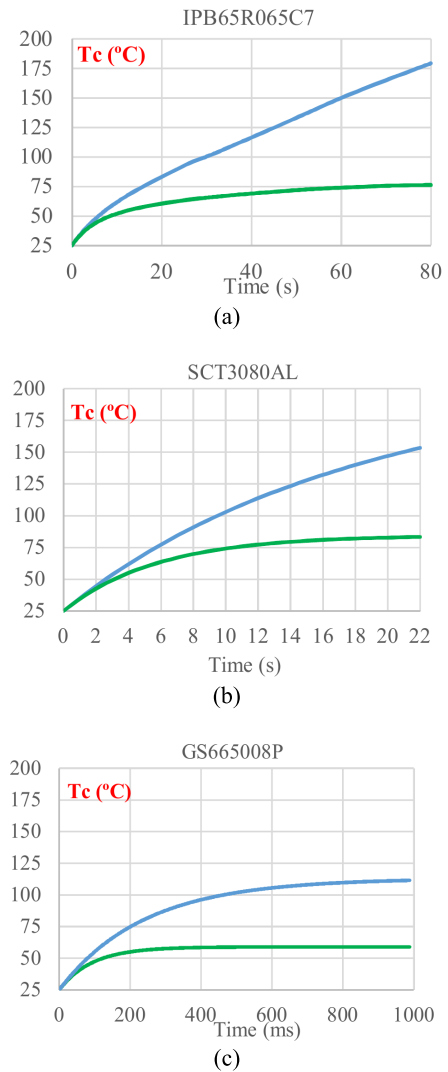


**FIGURE 6.** Case temperature  $T_c$  versus time with (green) and without (blue) heat sink for the chosen transistors: (a) Si, (b) SiC, and (c) GaN.

different thermal resistances involved in the heat transfer process:  $R_{\theta JC}$  (junction-to-case thermal resistance),  $R_{\theta TIM}$  (TIM thermal resistance),  $R_{\theta HSA}$  (heat sink to ambient thermal resistance),  $R_{\theta PCB}$  (PCB thermal resistance) and  $R_{\theta JA}$  (junction-to-ambient thermal resistance). The GaN device presents smaller  $R_{\theta JA}$  than Si and SiC, both with and without heat sink, and so, it will dissipate heat better. Fig. 6 shows the time evolution of case temperature  $T_c$  for the chosen transistors with and without heat sink when they are continuously switching (at 1 kHz and similar dissipated average power) during an enough time interval. The effect of the heat sink is clearly seen in all the graphs: every device experiences a much lower temperature increase with an external heat sink. Moreover, the GaN transistor shows significantly lower temperature increases than Si and SiC devices both with and without heat sink. As well, it shows times for stabilization temperature of up to one hundred times smaller than the other.

Finally, we have checked by simulation that the transistors switching times are in good agreement with the data in the

TABLE 4. Thermal resistances of Si, SiC and GaN transistors.

	$R_{\theta JC}$ (°C/W)	$R_{\theta PCB}$ (°C/W)	$R_{\theta TIM}$ (°C/W)	$R_{\theta HSA}$ (°C/W)	$R_{\theta JA}$ (°C/W)
Si	-	-	-	-	45
Si with heat sink	1.73	-	0.8	18	20.53
SiC	-	-	-	-	45
SiC with heat sink	0.86	-	1	8.6	10.46
GaN	-	-	-	-	24
GaN with heat sink	0.5	4.82	1.52	6.6	13.44

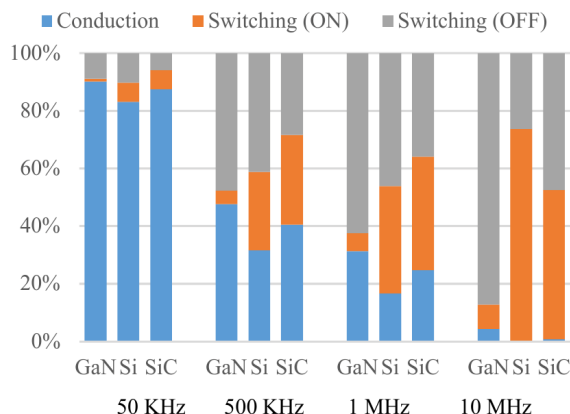


FIGURE 7. Percentage of energy dissipated in conduction, switching on and switching off over the total energy loss of each transistor (GaN, Si, SiC) for different frequencies.

datasheet. In fact, the Si and SiC transistors cannot switch fast enough beyond 10 MHz while the GaN transistor presents this limit at 100 MHz. Simulations have been performed at frequencies of 50KHz, 500 KHz, 1 MHz and 10 MHz and we have collected data of energy and power losses both in conduction and in switching turn-on and turn-off. Fig. 7 shows a diagram of the percentage of energy dissipated in conduction, switching on and switching off over the total energy loss of each transistor for different frequencies. As expected, switching losses increase with frequency. Fig. 8 shows a diagram of average power dissipation of each transistor for different frequencies. It can be observed that the power loss of the GaN transistor is smaller and, besides, it is more noticeable with frequency.

V. EXPERIMENTAL SETUP AND RESULTS OF THE GaN-BASED CONVERTER

In order to implement the converter, all its components have been chosen carefully taking into account the design considerations explained in Section 3 and seeking to obtain high efficiency in the system. Using components models as realistic as possible in simulation, we can estimate the influence of the real characteristics of the elements on the converter’s performances. The final selected GaN transistor is a GS61004B because it implies a good compromise between the  $R_{DS(on)}$  (15 mΩ) and the input capacitance  $C_{ISS}$  (295 pF) comparing it with other GaN transistors and, besides, it only costs about 6 \$. It has a  $BV_{DS}$  of 100 V which is sufficient for our application. We have opted for an Arduino Due to



FIGURE 8. Average power dissipation of each transistor (GaN, Si, SiC) for different frequencies.

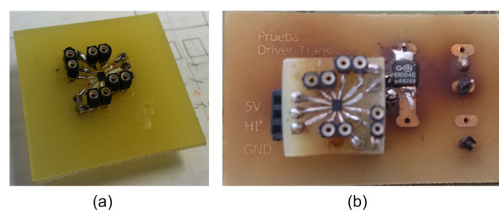


FIGURE 9. (a) The high-quality rework system used; (b) the gate driver shield built; (c) an additional board built to test the driver and the GaN transistor separately from the converter.

implement the PWM control. It is a microcontroller board based on the Atmel SAM3X8E ARM Cortex-M3 CPU, easy to use and with enough power for our application full enough. Since it runs at 3.3 V, a gate driver is needed to directly drive the transistor. We have searched a specific driver for GaN transistors, the LMG1205YFXR, which is a MHz gate driver whose high-side bias voltage is generated using a bootstrap technique and is internally clamped at 5 V, which prevents the gate voltage from exceeding the maximum gate-source voltage rating of the transistor.

Since our aim is to demonstrate the advantages of using GaN technology in a converter for a hybrid UAV, we have built a modular prototype. So we have made in an easier way the necessary changes and components substitutions that usually arise in a laboratory to achieve the goal. Since the driver is a 12-pin DSBGA (Die Sized Ball Gate Array) package very small (2 mm × 2 mm of body size) and difficult to solder, we have built a shield that allows different external configurations. Fig. 9(a) shows the driver shield. Fig. 9(b) shows the Printed Circuit Board (PCB) we have also built to test the operation of the driver with the GaN transistor separately from the converter. For the load, we made an arrangement that consisted of five rows of four precision military grade resistors each one. Individually one of these resistors could withstand a maximum of 3 W. Therefore, each row could dissipate up to 12W. The set allowed to connect the desired rows, obtaining a consumption of 12 W per row connected. The inductor, diode and capacitor of the converter have been mounted onto other PCB. Finally, we substituted the PCB with the GaN transistor for another with some transistors in

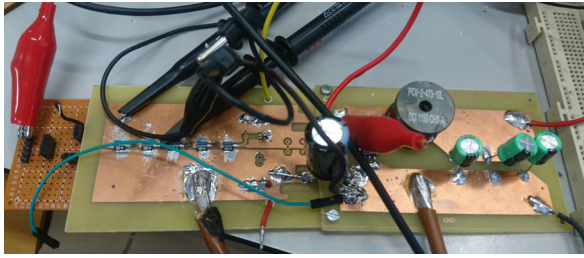


FIGURE 10. Final prototype for the proof-of-concept of the GaN converter.

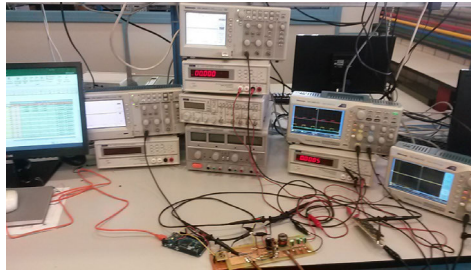


FIGURE 11. Experimental setup for testing the converter.

parallel for more flexibility. Fig. 10 shows the final prototype that serves as proof-of-concept of the proposed GaN-based converter. In this final prototype we have also used three  $68 \mu\text{F}$  electrolytic capacitors in parallel, a power inductor of  $47 \mu\text{H}$  and a diode VS-12CWQFN-M3.

It has been checked the operation of the converter by several experimental setups. Firstly, as we mentioned before, we have tested each module separately and, afterwards, the whole system.

In a first step, we have checked the correct response of the driver connected to some tests boards: one, with a low-side transistor and other, with a high-side transistor. Tests were carried out for a frequency range checking the gate-source signal on the oscilloscope. In addition, we tried with different values of the bootstrap and bypass capacitors and external resistances to the gate of the transistor to observe the response and the gate voltage oscillations due to parasitic inductances. We have checked frequencies up to 2 MHz.

The first tests showed the open-loop converter worked properly. Fig. 11 shows the experimental setup to test the converter. We varied the duty cycle and the operation frequency. Nevertheless there were ringing effects in the circuit and they became more serious when the input voltage increased. So, as a precaution, we tried to solve the ringing effects making initial measurements at low power, with small values of input (around 12 V) and output voltage (around 4 V). We obtained measurements of power efficiency for different values of switching frequency (from 60 kHz to 200 kHz) and they kept all beyond 91% and more or less constant. Then we decided to fix the frequency at 100 kHz for the following tests. In order to illustrate ringing effect and how it could damage the GaN transistor Fig. 12(a) shows the oscillations observed in the gate-source voltage waveform around the switching instants, when source voltage changes at a faster rate. Since

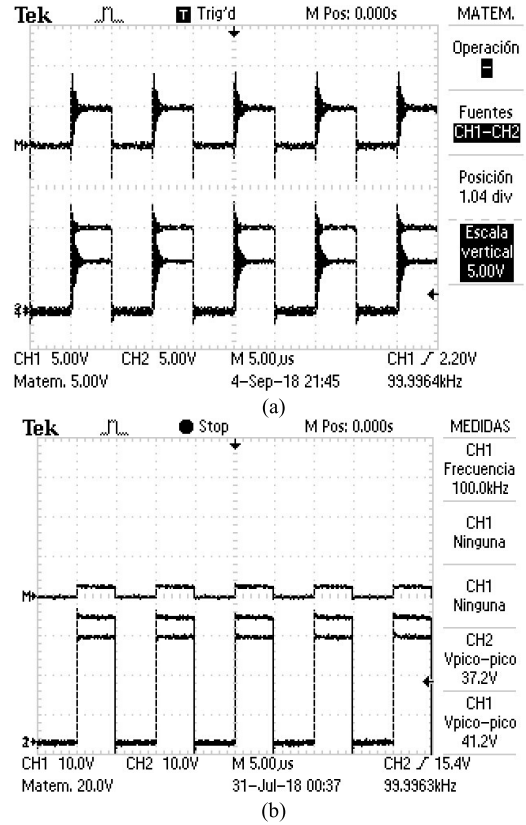


FIGURE 12. Gate voltage (CH1 or channel 1), source voltage (CH2 or channel 2) and gate-source voltage (CH1-CH2) when (a) no anti-ringing measures are applied; (b) our anti-ringing measures are applied.

the maximum rating for  $V_{GS}$  is  $(-10 \text{ V}, +7 \text{ V})$  and for a transient of  $1 \mu\text{s}$   $V_{GS(\text{transient})}$  is  $(-20\text{V}, +10 \text{ V})$ , the oscillation when the transistor turns on is potentially dangerous. In order to reduce ringing effect, we applied an optimal combination of measures: two external gate resistors between the driver and the gate of the transistor ( $R_{G(\text{on})}$  and  $R_{G(\text{off})}$  of  $47 \Omega$ ) and a snubber circuit between the source of the transistor and ground ( $R_{\text{snubber}} \approx 35 \Omega$  and  $C_{\text{snubber}} \approx 2.2 \text{ nF}$ ). Fig. 12(b) shows how our anti-ringing measures make  $V_{GS}$  present good behavior even with high voltages at the input (37.2 V in the figure). These anti-ringing measures reduce the total efficiency of the converter, but we think they are necessary since our converter is intended for an aeronautical application. For this same reason, as additional safety measure, we have added a 5 V zener diode between gate and source of the transistor, although it also contributes to power losses.

Then, the following step has been to check the operation of the converter in open loop and for high power. We have taken initial data by varying the input with voltage values between 22 V and 50 V for current through the load of a 1 A. Table 5 shows the different measurements taken for this case as well as the efficiency. The circuit works properly: with the theoretical value of  $D$  to give a 12 V output, although the converter is in open loop configuration, it provides 11.5 V approximately in all cases. The values of efficiency are also satisfactory, regardless of the incorporated safety measures

TABLE 5. Open loop measurements for 1 A through the load.

$V_i$ (V)	$I_i$ (A)	$V_o$ (V)	$I_o$ (A)	$\eta$ (%)
21.998	0.51	11.561	0.9595	98.88
23.989	0.48	11.563	0.96	96.40
28.005	0.39	11.407	0.946	98.80
32,004	0.36	11.508	0.955	95.39
33	0.35	11.542	0.957	97.02
33.999	0.33	11.506	0.954	97.83
35	0.33	11.582	0.96	96.27
35.987	0.32	11.501	0.953	96.69
36.999	0.30	11.569	0.96	100.0
38.012	0.30	11.533	0.956	96.68
38.99	0.30	11.564	0.96	94.91
40.003	0.30	11.588	0.96	92.70
40.998	0.27	11.528	0.955	99.46
41.994	0.27	11.414	0.946	95.23
45.993	0.24	11.456	0.949	98.49
50.009	0.24	11.46	0.95	90.71

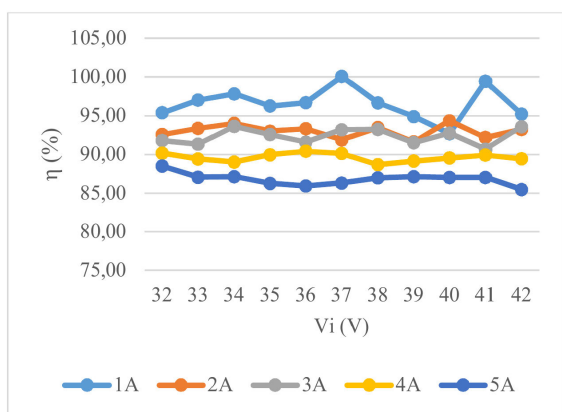


FIGURE 13. Open-loop converter efficiency versus input voltage for values of output current.

(which increase power losses) and the fact that the board is not optimized yet to reduce the parasitic effects of connections. In a final and integrated prototype, the expected efficiency will be even better.

We have also taken a series of measurements for different values of output current. The numerical results allow verifying the correct operation of the circuit with the increase in power. The converter shows a small decrease in efficiency with the increase of power as well as a small decrease in the reduction ratio with respect to the theoretical one for each D value. To illustrate the most significant results we present the Fig. 13, which shows the efficiency curve interpolating the points obtained including an input voltage sweep from 32 V to 42 V in steps of 1 V and for values of the input current from 1 A to 5 A with 1 A step increment. We can observe clearly how the efficiency is very high for small power values and, as expected, it decreases when the operating power increases.

Finally, we have checked the operation of the converter in closed loop, that is, in its normal operation mode inside the aircraft. In this case, it is necessary to use a voltage divider to scale and connect the converter output safely to one of the analog inputs of the Arduino Due (the maximum voltage input that can be read is 3.3 V). The two resistances

TABLE 6. Closed loop measurements of the converter.

$V_i$ (V)	$I_i$ (A)	$V_o$ (V)	$I_o$ (A)	$\eta$ (%)
32.004	0.39	11.949	0.994	95.16
32.004	0.39	11.95	0.996	95.36
35.987	0.36	12.05	1.005	93.48
40.003	0.33	12.14	1.01	92.88
32.004	0.78	11.894	1.971	93.91
35.987	0.69	11.95	1.97	94.81
36.004	0.69	12.02	2.01	97.25
40.003	0.66	12.1	2.025	92.81
32.004	1.18	11.87	2.95	92.72
35.987	1.12	12.15	3.03	91.34
40.003	0.99	12.015	3.01	91.32
32.004	2.17	12.195	5.062	88.89
35.987	1.9	12.046	5.01	88.26
40.003	1.75	12.05	5.01	86.24

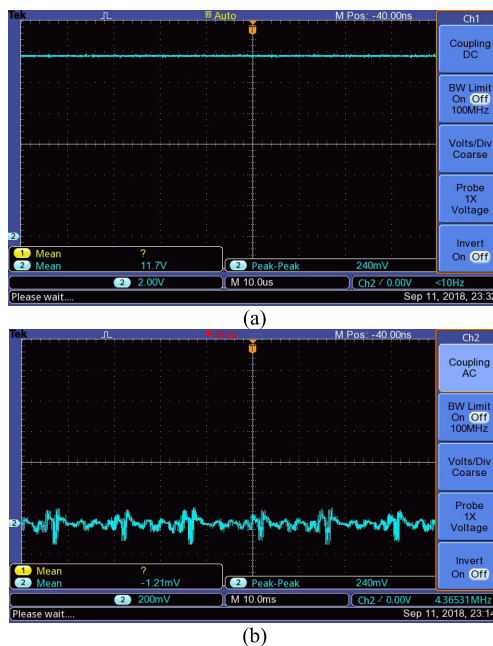
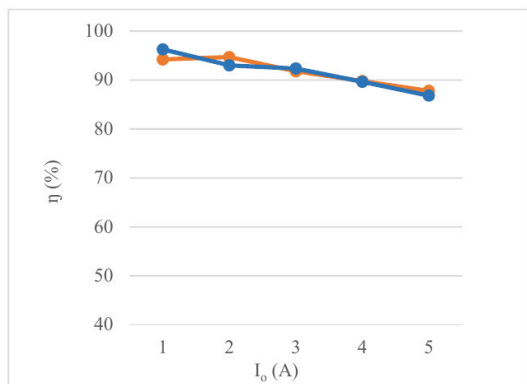


FIGURE 14. Output voltage in the oscilloscope with (a) CC coupling (b) AC coupling.

used for the divider are 22 kΩ and 4.7 kΩ. Table 6 shows some significant measurements. In closed loop configuration, as expected, we have observed that the errors in the output voltage and current are much smaller than in the open loop case. The output is constantly being corrected, by means of the continuous modification of the D value, with satisfactory load regulation and line regulation (between 0.8% and 2.5% in any case).

The converter has also shown a good behavior regarding the output voltage ripple. By way of illustration, Fig. 14(a) shows an example of the output voltage measured in an oscilloscope with CC coupling. Fig. 14(b) shows the output voltage in AC coupling in order to highlight the output voltage ripple (240 mV<sub>pp</sub>).

Fig. 15 shows the converter efficiency for a 36 V input in open-loop and closed-loop configurations. In both cases, with the increase in the load current, the efficiency decreases due to the increase in the conduction dissipation of the components.



**FIGURE 15.** Comparison of the converter efficiency for a 36 V input in open-loop (blue line) and closed-loop (orange line) configurations.

Efficiency results are very promising. They range between 85% and 99% despite the fact that we have added a snubber and resistances between the gate driver and the transistor to alleviate the ringing effect. We have also added a zener diode as safety measure to protect the transistor and a 220  $\mu\text{F}$  input capacitor to reduce the ripple voltage amplitude seen at the input of the converter (although its equivalent series resistance should have been lower). Obviously, all these additional components contribute to decrease the overall efficiency. In addition, even though the converter is not optimized yet and it is a proof-of-concept prototype, it represents a technological demonstrator of the benefit of applying GaN technology in power converters for aircrafts.

## VI. CONCLUSION AND FUTURE WORK

In this work we have explored the use of SiC and GaN technologies versus Si technology in a converter for a small hybrid UAV, checking their advantages and disadvantages in a real case of aeronautics. After theoretical studies and simulations, GaN technology has turned out the best option because the power switches present these properties: lower size, weight and a combination of lower switching and conduction losses which favors higher efficiencies. Therefore, a GaN-based buck converter was designed and implemented. Since GaN power switches technology is not a mature technology, its benefits are not fully realized if they are treated as drop-in replacements for Si devices. It is necessary to conduct research in order to optimize the properties of the GaN switches and minimize size and costs of cooling systems and auxiliary circuit components.

The converter developed has been tested experimentally in the laboratory. Results confirm its proper functioning. We can say that our design already fulfils most of requirements. It is able to provide 12 V as regulated output from an input voltage in the range of 32 V to 40 V and an output power up to 60 W with small line and load regulations and a high efficiency (in the range of 85% up to over 99%). These promising efficiency results have been obtained even though the built converter is not optimized regarding integration and

minimization of connections. Based on the evidence found in this work, the final prototype is sure to meet the size and weight requirements.

In the future we intend to integrate all the components in a board reducing the effect of parasitic capacitances and inductances and mitigating the ringing phenomenon without noticeably decreasing the efficiency. One possible improvement for closed loop operation would be the replacement of the Arduino Due with a dedicated controller, designed and manufactured specifically for converter applications, where the transient response was optimized to reduce the possible losses. We will also extend the number and coverage of the experiments to demonstrate the performances of the system, for example, sweeping the switching frequency and studying the issue of electromagnetic interference (EMI). Finally, we aspire to adapt the prototype to the current UAV being developed and achieve its full operation.

## REFERENCES

- [1] Federal Aviation Administration, Washington, DC, USA. (2016). *FAA Aerospace Forecast Fiscal Years 2016–2036*. [Online]. Available: [https://www.faa.gov/data\\_research/aviation/aerospace\\_forecasts/media/fy2016-36\\_faa\\_aerospace\\_forecast.pdf](https://www.faa.gov/data_research/aviation/aerospace_forecasts/media/fy2016-36_faa_aerospace_forecast.pdf)
- [2] PwC. (2016). *PwC Global Report on the Commercial Applications of Drone Technology*. [Online]. Available: <https://www.pwc.pl/pl/pdf/clarity-from-above-pwc.pdf>
- [3] T. Lei, Z. Yang, Z. Lin, and X. Zhang, "State of art on energy management strategy for hybrid-powered unmanned aerial vehicle," *Chin. J. Aeronaut.*, vol. 32, no. 6, pp. 1488–1503, Jun. 2019.
- [4] E. Bataller-Planes, N. Lapena-Rey, J. Mosquera, F. Ortí, J. Á. Oliver, Ó. García, F. Moreno, J. Portilla, Y. Torroja, M. Vasic, S. C. Huerta, M. Trocki, P. Zumel, and J. A. Cobos, "Power balance of a hybrid power source in a power plant for a small propulsion aircraft," *IEEE Trans. Power Electron.*, vol. 24, no. 12, pp. 2856–2866, Dec. 2009.
- [5] A. Savvaris, Y. Xie, K. Malandrakis, M. Lopez, and A. Tsourdos, "Development of a fuel cell hybrid-powered unmanned aerial vehicle," in *Proc. 24th Medit. Conf. Control Autom. (MED)*, Jun. 2016, pp. 1242–1247.
- [6] B. Lee, S. Kwon, P. Park, and K. Kim, "Active power management system for an unmanned aerial vehicle powered by solar cells, a fuel cell, and batteries," *IEEE Trans. Aerosp. Electron. Syst.*, vol. 50, no. 4, pp. 3167–3177, Oct. 2014.
- [7] J. Millán, P. Godignon, X. Perpiñà, A. Pérez-Tomás, and J. Rebollo, "A survey of wide bandgap power semiconductor devices," *IEEE Trans. Power Electron.*, vol. 29, no. 5, pp. 2155–2163, May 2014.
- [8] A. Lidow, J. Strydom, M. Rooij, and D. Reusch, *GaN Transistors for Efficient Power Conversion*, 2nd ed. New York, USA: Wiley, 2015.
- [9] A. Bindra, "Wide-Bandgap-Based power devices: Reshaping the power electronics landscape," *IEEE Power Electron. Mag.*, vol. 2, no. 1, pp. 42–47, Mar. 2015.
- [10] R. Chu, Y. Cao, M. Chen, R. Li, and D. Zehnder, "An experimental demonstration of GaN CMOS technology," *IEEE Electron Device Lett.*, vol. 37, no. 3, pp. 269–271, Mar. 2016.
- [11] M. Ishida, T. Ueda, T. Tanaka, and D. Ueda, "GaN on Si technologies for power switching devices," *IEEE Trans. Electron Devices*, vol. 60, no. 10, pp. 3053–3059, Oct. 2013.
- [12] Z. Liu, Y. He, L. Yang, and J. Han, "Control techniques of tilt rotor unmanned aerial vehicle systems: A review," *Chin. J. Aeronaut.*, vol. 30, no. 1, pp. 135–148, Feb. 2017.
- [13] M. Vargas, S. Esteban, C. Bordons, X. Blasco, L. Buss-Becker, A. Cuerva, C. Castillo, S. García-Nieto, J. Justo, O. López, J. Macías, J. Martínez, J. L. Mora, J. Normey, M. Ortega, and G. Raffo, "Development of unmanned convertible aircraft for rapid and efficient deployment in emergency situations: Project EMERGENTIA," in *International Forum DRONE Berlin*. DEMACH Event- und Veranstaltungs GmbH: Berlin, Germany, Sep. 2017.

[14] S. Esteban, C. Bordons, X. Blasco, L. Buss-Becker, A. Cuerva, C. Castillo, S. García-Nieto, J. Justo, O. López, J. Macías, J. Martínez, J. L. Mora, J. Normey, M. Ortega, G. Raffo, and M. Vargas, “Desarrollo de una aeronave convertible no-tripulada para despliegue rápido y eficiente en situaciones de emergencia: Proyecto EMERGENTIA,” in *Proc. Conf. CivilDRON*, Madrid, Spain, Jan. 2018, pp. 1–21.

[15] N. Mohan, T. M. Undeland, and W. P. Robbins, *Power Electronics: Converters, Applications, and Design*, 2nd ed. Hoboken, NJ, USA: Wiley, 1995.

[16] S. Debnath, J. Qin, B. Bahrani, M. Saeedifard, and P. Barbosa, “Operation, control, and applications of the modular multilevel converter: A review,” *IEEE Trans. Power Electron.*, vol. 30, no. 1, pp. 37–53, Jan. 2015.

[17] T. P. Chow, I. Omura, M. Higashiwaki, H. Kwarada, and V. Pala, “Smart power devices and ICs using GaAs and wide and extreme bandgap semiconductors,” *IEEE Trans. Electron Devices*, vol. 64, no. 3, pp. 856–873, Mar. 2017.

[18] A. Hassan, Y. Savaria, and M. Sawan, “GaN integration technology, an ideal candidate for high-temperature applications: A review,” *IEEE Access*, vol. 6, pp. 78790–78802, 2018.

[19] E. O. Johnson, “Physical limitations on frequency and power parameters of transistors,” *RCA Rev.*, vol. 26, pp. 163–177, Jun. 1965.

[20] R. W. Keyes, “Figure of merit for semiconductors for high-speed switches,” *Proc. IEEE*, vol. 60, no. 2, p. 225, Feb. 1972.

[21] B. J. Baliga, “Semiconductors for high-voltage, vertical channel field-effect transistors,” *J. Appl. Phys.*, vol. 53, no. 3, pp. 1759–1764, Mar. 1982.

[22] B. J. Baliga, “Power semiconductor device figure of merit for high-frequency applications,” *IEEE Electron Device Lett.*, vol. 10, no. 10, pp. 455–457, Oct. 1989.

[23] W. G. Bi, H. C. Kuo, P. C. Ku, and B. Shen, *Handbook of GaN Semiconductor Materials and Devices*, 1st ed. Boca Raton, FL, USA: CRC Press, 2017.

[24] K. Shenai, “The figure of merit of a semiconductor power electronics switch,” *IEEE Trans. Electron Devices*, vol. 65, no. 10, pp. 4216–4224, Oct. 2018.



**JOSÉ LUIS MORA-JIMÉNEZ** received the M.S. and Ph.D. degrees in industrial engineering from University of Seville (US), Spain, in 1992 and 2001, respectively. He is currently an Associate Professor with the Department of Electronic Engineering, US. His current research areas are modeling and control of power converters, multilevel converters, and sensor-less motor drives.



**ALEJANDRO REMUJO** received the B.S. degree in aerospace engineering from the University of Seville, Spain, in 2018. He is currently pursuing the M.S. degree in space and astronautical engineering with the University La Sapienza, Rome, Italy. His research interests include space systems, power electronics, and sensors.



**JOAQUÍN SORIANO** received the B.S. degree in aerospace engineering from the University of Seville, Spain, in 2019. He is currently pursuing the M.S. degree in space and astronautical engineering from the University La Sapienza, Rome, Italy. His research interests include electronics and avionics, space systems, orbital mechanics, and propulsion.



**JUANA M. MARTÍNEZ-HEREDIA** (Member, IEEE) received the M.S. and Ph.D. degrees in telecommunications engineering from the University of Seville (US), Spain, in 1999 and 2006, respectively. Since 1999, she has been with the Department of Electronic Engineering, USA, where she is currently an Associate Professor. Her research interests include low-voltage low-power analog circuit design, analog and mixed-signal design, and the design of circuits for aircrafts and UAVs.



**FRANCISCO COLODRO** received the M.S. degree in telecommunications engineering from the University of Vigo, Spain, in 1992, and the Ph.D. degree from the University of Seville (US), Spain, in 1997. He is currently a Senior Lecturer with the Department of Electronic Engineering, USA. His research interests include analog-to-digital and digital-to-analog conversion, sigma-delta modulators, and electronic circuits and systems with application to control, aeronautics, and communications.



**SERGIO ESTEBAN** received the B.S. and M.S. degrees in aerospace engineering from the Missouri Science and Technology University, in 1999 and 2002, respectively, and the Ph.D. degree from University of Seville (US), in 2011. Since 2007, he has been an Associate Professor with the Department of Aerospace Engineering, US. His research interests include aircraft and UAV design, and nonlinear control, and the guidance of aerospace vehicles.

...